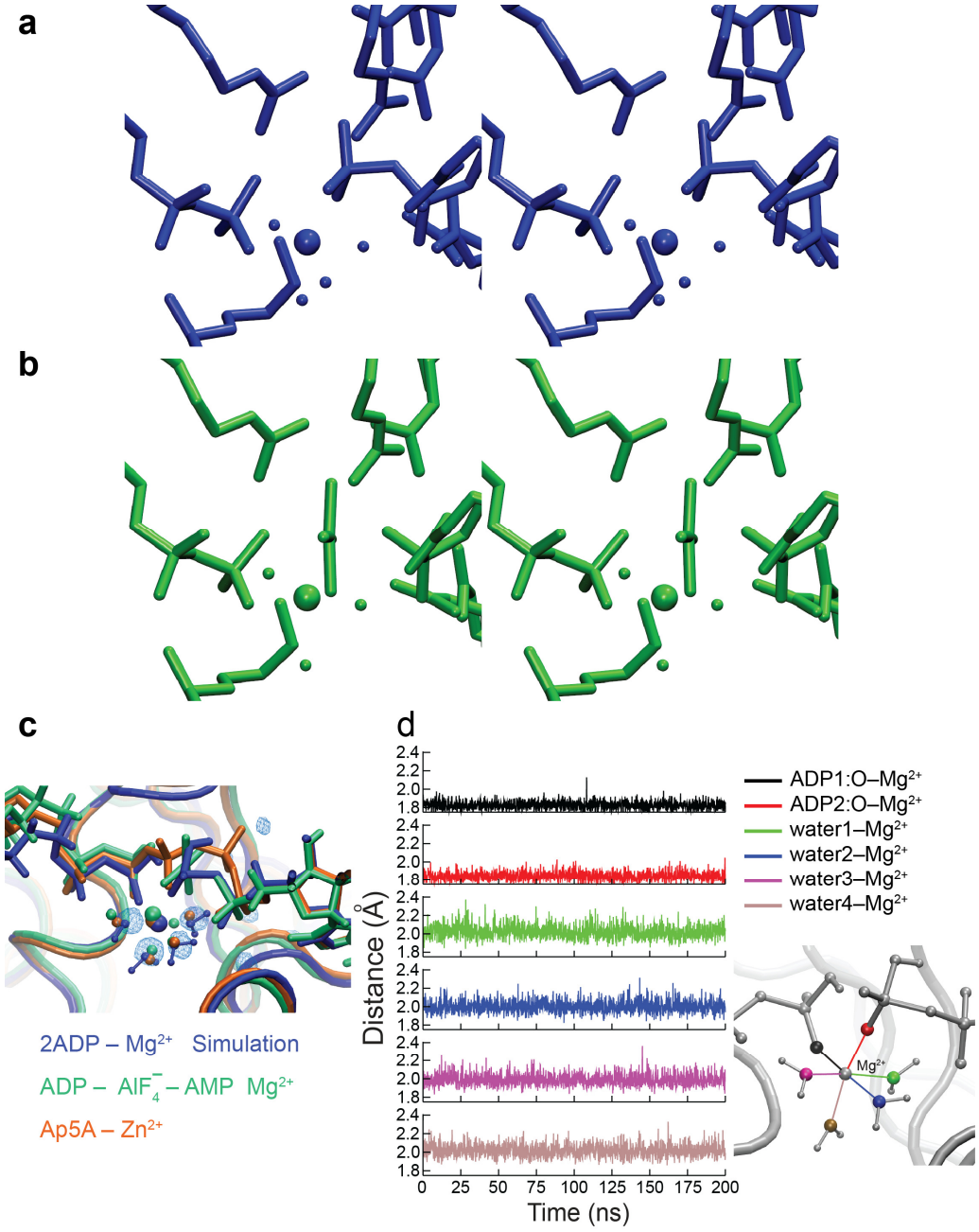

Supplementary Figure 1

Magnesium coordination and water in the active site.

a,**b**. Stereo view of Fig. 1e showing detailed active-site interactions for the Mg^{2+}–ADP–ADP (blue) and Mg^{2+}–ADP–AMP–AlF_4^- structures (green). **c**. Superimposition of X-ray structures (PDB 3SR0 and 2RGX), and a representative snapshot from the MD simulation. The positions of the divalent cation, water molecules, and the nucleotide oxygen atoms in the simulation are in full agreement with the corresponding atoms in the crystal structures. The blue wireframe surface represents the isosurface of value 0.99 for the fractional occupancy of the water oxygen atoms during a typical MD simulation. **d**. Octahedral coordination of the Mg^{2+} ion in the active site monitored during a 200 ns MD simulation of AAdk bound to Mg^{2+}–ADP–ADP. The coordination partners are depicted on the structure and the corresponding time-dependent Mg^{2+}–O distances during the MD simulation are shown.

1. Henzler-Wildman, K.A. et al. Intrinsic motions along an enzymatic reaction trajectory. Nature 450, 838-44 (2007)

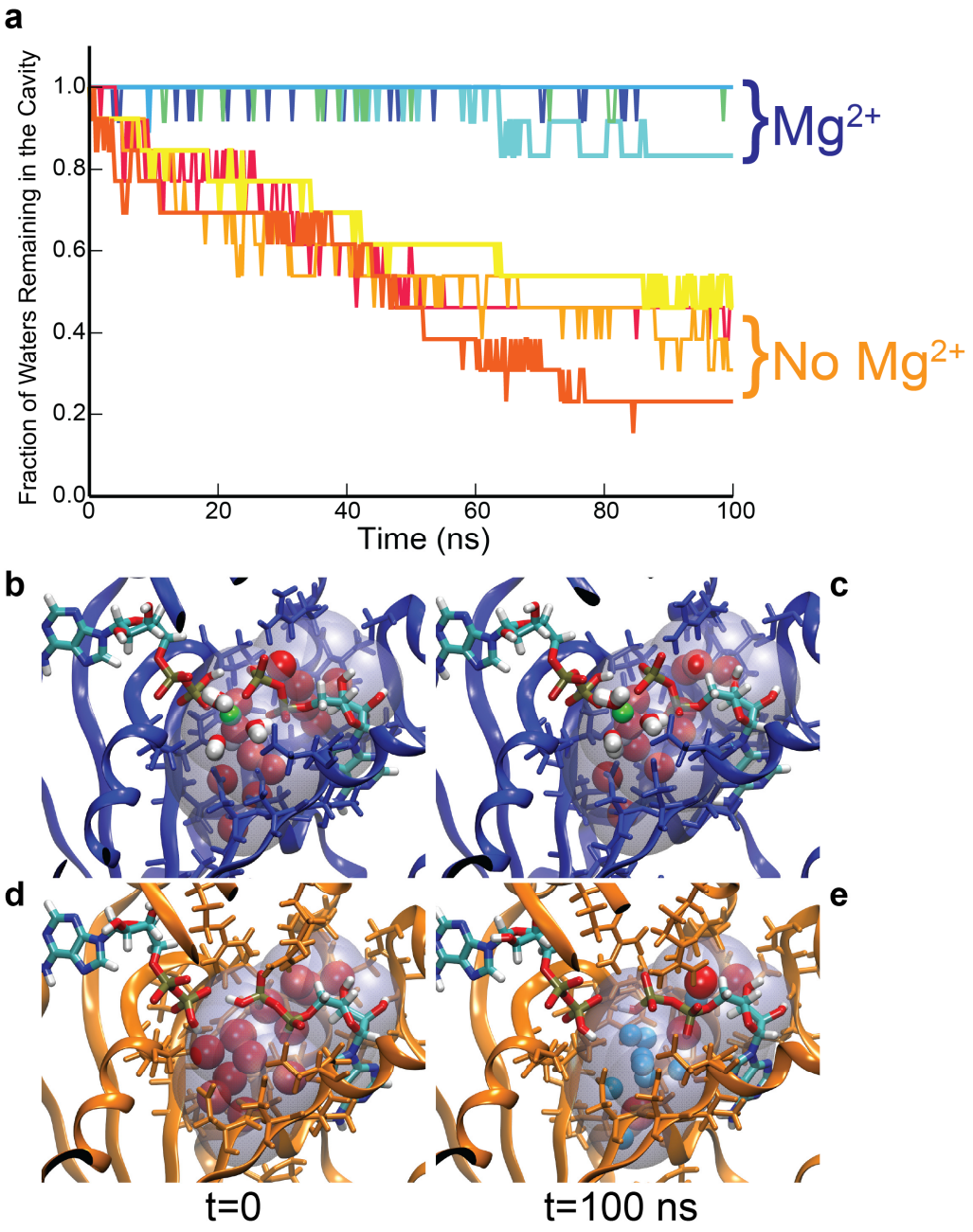

Supplementary Figure 2

Mg^{2+} prevents water molecules trapped in the active site from exchanging with bulk water.

(a–e) Behavior of all water molecules in the active-site cavity for 100 ns MD simulations of AAdk bound to ADP–ADP with and without Mg^{2+}. **a**. The fraction of the water molecules present in the active site at the beginning of the simulation, that are still inside the cavity at time t is plotted for four simulations in the presence (dark blue to green) and absence (red to yellow) of Mg^{2+}. The cavity considered for the analysis is displayed in the structures in panels **b**–**e**. The water oxygen atoms initially present in the cavity are displayed as large red spheres and the four water molecules coordinating Mg^{2+} are shown in red and white sticks. In the simulations with Mg^{2+} (**b** and **c**), all water molecules stay in the cavity (see also Movie 1). In the simulations without Mg^{2+} (**d** and **e**), the water molecules in the pocket progressively diffuse out, exchanging with bulk water and are substituted by other water molecules (depicted as cyan spheres). The average number of water molecules in the cavity is constant in all simulations.

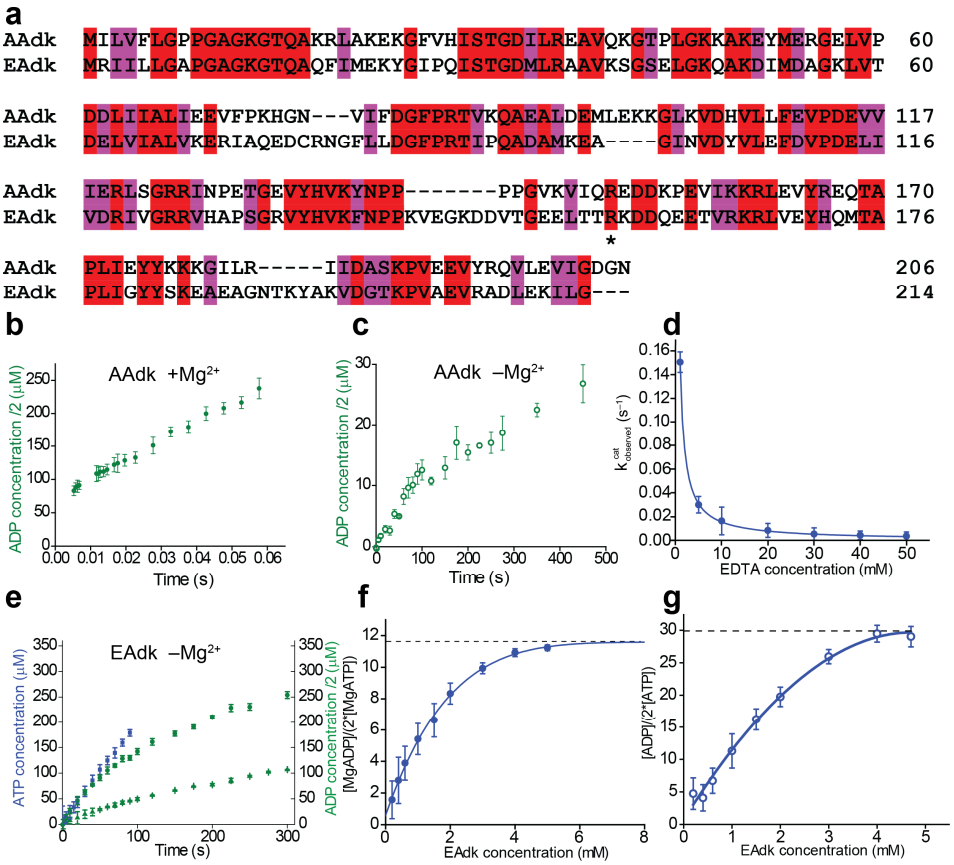

Supplementary Figure 3

Comparison of AAdk and EAdk sequences and pre-steady-state kinetics with and without Mg^{2+}, and determination of the on-enzyme equilibrium for EAdk.

a. Sequence alignment of adenylate kinase from *Aquifex aeolicus* (AAdk) and *Escherichia coli* (EAdk). Identical residues are colored in red and similar residues in purple. To avoid confusion, the residue numbering used in the present manuscript refers always to the AAdk sequence. For example, when we indicate R150 (marked with * in the sequence), we are in fact referring to R150 for AAdk and R156 for EAdk. **b**. Quench-flow experiments performed in the forward direction with 100 μM AAdk, 4 mM ATP and AMP, and 8 mM Mg^{2+}. **c**. Quench-flow experiments performed in the forward direction with 25 μM AAdk, 4 mM ATP and AMP, and 50 mM EDTA to remove Mg^{2+} contamination. Data shows that the rate-limiting step of AAdk turnover, like EAdk (Fig. 3), is lid-opening in the presence of Mg^{2+} **(b)** and phosphoryl transfer in the absence of Mg^{2+} **(c)**. This highlights the mechanistic similarity between the two proteins, which is further bolstered by the nearly identical active site in crystal structures of AAdk (PDB 2RGX) and EAdk (PDB 1AKE) in complex with the bi-substrate inhibitor Ap5A. **d**. EDTA titration of EAdk + 4 mM ADP complex monitored by a change in k_{cat} for the reverse reaction. Due to the fact that 50 mM EDTA was needed to remove trace elements of divalent cations, all “no divalent cation” kinetics experiments were performed with 50 mM EDTA to ensure that the measured rates were not influenced by minor divalent cation contamination. **e**. Quench-flow experiments performed at different EAdk concentrations in the forward (25 and 100 μM) and reverse (485 μM) directions with 4 mM ATP and AMP or 4 mM ADP. 50 mM EDTA was present in all experiments to remove residual Mg^{2+}. Data show the same behavior as at low EAdk concentration (Fig. 3), but fitting was less reliable because the back reaction had to be accounted for, due to the increased amount of generated product. **f,g**. Determination of the on-enzyme equilibrium in the presence of Mg^{2+} (**f**, 600 μM of MgADP) and absence of Mg^{2+} at (**g**, 600 μM ADP + 50 mM EDTA). The [ADP]/2*[ATP] ratio was measured as a function of increasing concentration of EAdk. At low enzyme concentration most nucleotides are free, and the ADP to ATP ratio mainly reflects equilibrium in solution. When the plateau is reached, all nucleotides are bound and the corresponding [ADP]/2*[ATP] ratio reflects the on-enzyme equilibrium. In the presence of Mg^{2+}, fitting it to a generalized hyperbola (y = a - b/(1 + c*x)^(1/d)) yielded an equilibrium value of 11.6 ± 0.7, which is in good agreement with the number obtained from kinetic experiments (see Fig. 3a). In the absence of Mg^{2+} the equilibrium was shifted even further, yielding a value of 29 ± 1.

1. Henzler-Wildman, K.A. et al. Intrinsic motions along an enzymatic reaction trajectory. *Nature* **450**, 838-44 (2007).
2. Muller, C.W. & Schulz, G.E. Structure of the Complex between Adenylate Kinase from Escherichia-Coli and the Inhibitor Ap5a Refined at 1.9 a Resolution - a Model for a Catalytic Transition-State. *Journal of Molecular Biology* **224**, 159-177 (1992)

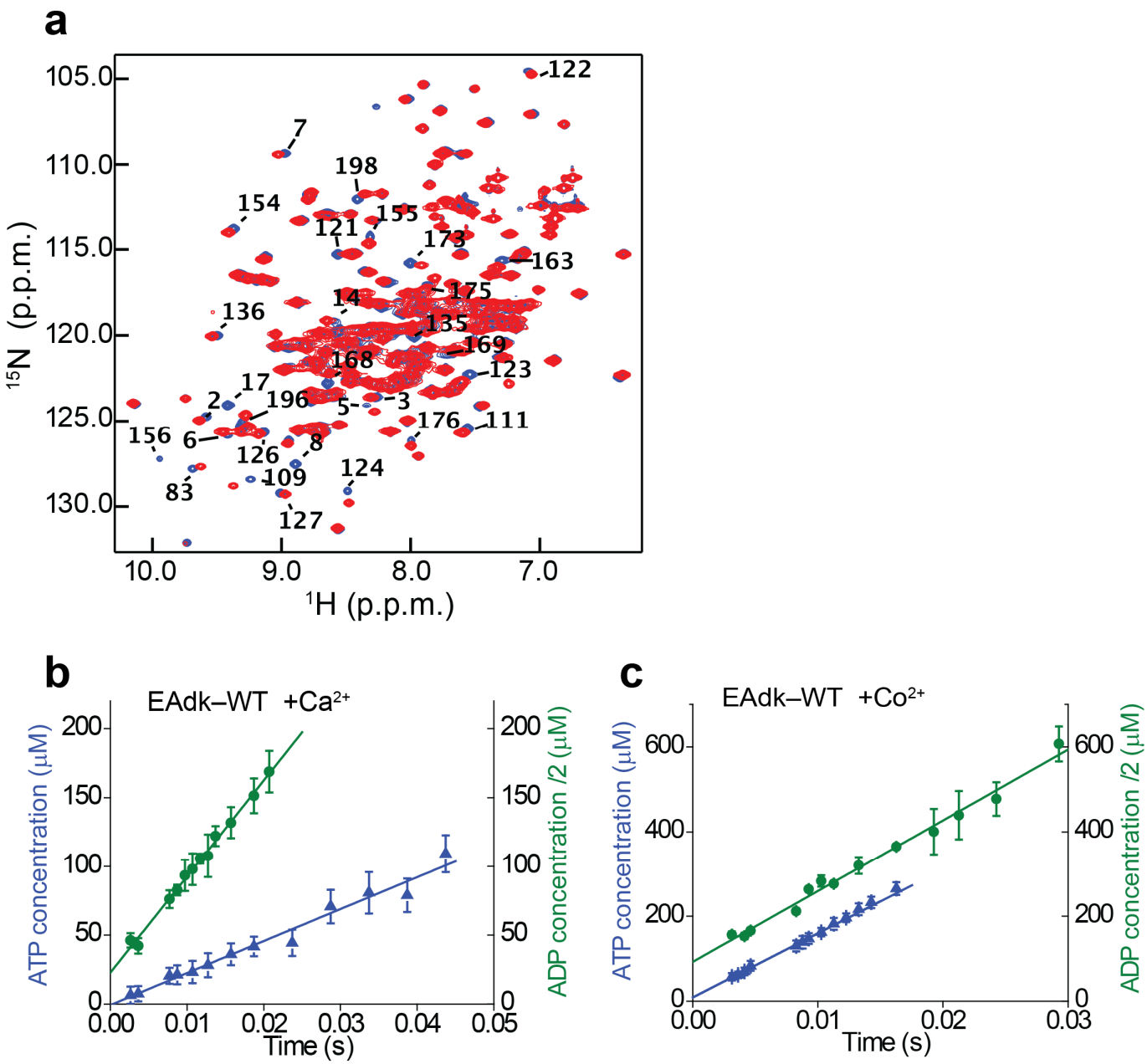

Supplementary Figure 4

Effect of the nature of the divalent cation on structure and kinetics.

a. The overlay of [^{1}H-^{15}N]-TROSY-HSQC spectra of EAdk with saturating concentrations of Mg^{2+} (blue) or Ca^{2+} (red) and saturating concentrations of nucleotides shows only minor chemical shifts changes indicating that the bound structures are very similar. The NMR experiments were collected with 2 mM EAdk, 20 mM ADP, and either 20 mM Mg^{2+} or 20 mM Ca^{2+}. **b,c**. Pre-steady-state kinetics of EAdk measured by quench-flow at 25 °C in the forward (green) and reverse direction (blue) with different divalent ions to obtain the rate constants in Table 2. **b**. 25 μM EAdk, 4 mM ATP and AMP, and 8 mM $CaCl_2$ in the forward reaction, and 100 μM EAdk and 4 mM ADP and $CaCl_2$ in the reverse direction (blue). **c**. 100 μM EAdk, 4 mM ATP and AMP, and 8 mM $CoCl_2$ in the forward direction and 100 μM EAdk and 4 mM ADP and $CoCl_2$ in the reverse direction. For Ca^{2+} and Co^{2+}, P-transfer is rate limiting in the reverse reaction, whereas lid-opening is rate limiting in the forward reaction (burst represents P-transfer).

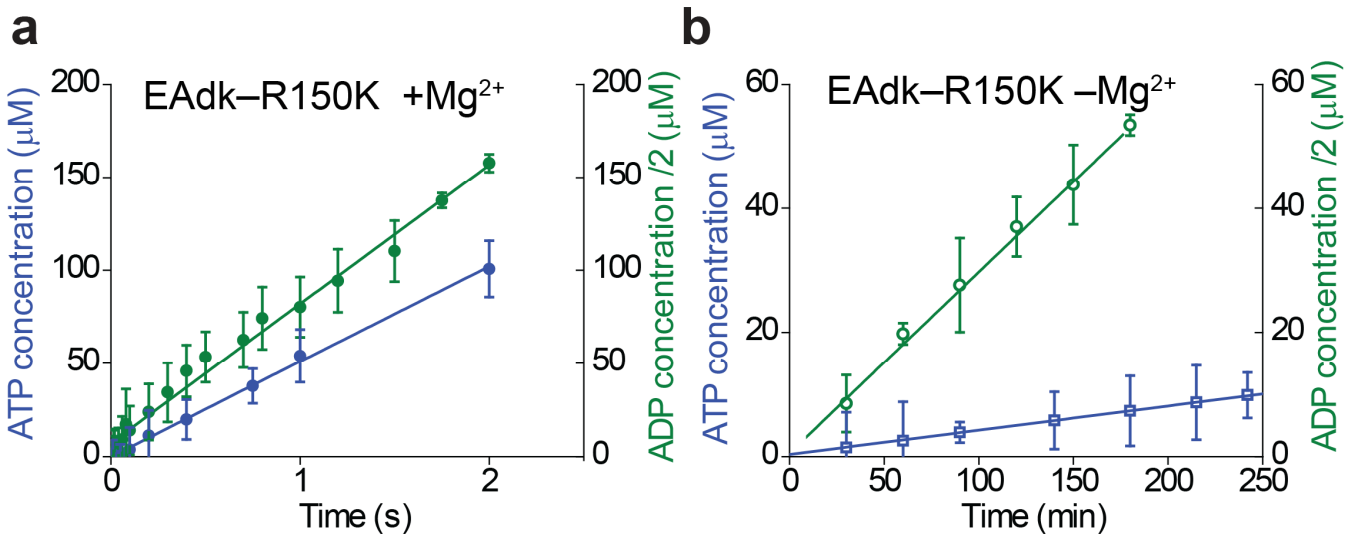

Supplementary Figure 5

Pre-steady-state kinetics measurements of EAdk R150K at 25 ℃.

a. Quench-flow experiments performed with 100 μM EAdk–R150K and 4 mM MgAMP + 4 mM MgATP in the forward direction and 100 μM EAdk–R150K and 4 mM MgADP in the reverse direction. **b**. 100 μM EAdK–R150K, 4 mM ATP + 4 mM AMP, and 50 mM EDTA in the forward direction and 100 μM EAdK-R150K, 4 mM ADP, and 50 mM EDTA in the reverse direction. For R150K, P-transfer is rate limiting in both directions with and without Mg^{2+}.

Metal	Radius (Å)	Charge (e)	Charge Density (e^2/ Å)	Turnover (s^{-1})
Li^+	0.9	1	1.11	0.5 ± 0.05
Ca^{2+}	1.14	2	3.51	12 ± 4
Mn^{2+} (hs)	0.97	2	4.12	55 ± 10
Mg^{2+}	0.86	2	4.65	230 ± 15*
Co^{2+} (hs)	0.885	2	4.52	140 ± 16
Ni^{2+}	0.83	2	4.82	90 ± 20

Supplementary Table 1: Turnover rate with different metal cofactors.
Turnover rate constants for EAdk at 25 °C with divalent metal cofactors was measured in the reverse direction (see also Fig. 5a). For all metals except Mg^{2+}, P-transfer is rate limiting. The EAdk turnover rates appear to correlate with the charge density of the metal cofactor.
* the rate-determining step for turnover with Mg^{2+} is the lid-opening conformational change. hs stands for high spin.

wild-type EAdk							EAdk R150K
	MgADP		CaADP		MgAp5A		MgADP
BMRB ID	19091		19090		4350		19093
k_{ex} (s^{-1})	1630 ± 30		2870 ± 160		965 ± 30		1500 ± 30
p_{major}	0.87 ± 0.05		0.87 ± 0.05		0.95 ± 0.05		0.80 ± 0.05
k_{open} (s^{-1})	210 ± 80		370 ± 140		100 ± 50		300 ± 75

Supplementary Table 2: Analysis of relaxation dispersion profiles.
Fitted parameters from ^{15}N-TROSY CPMG relaxation dispersion profiles recorded at 25 °C. Data were collected for 2 mM WT-EAdk or R150K mutant in presence of 20 mM MgADP, CaADP, or 5 mM MgAp5A. Data recorded at 600 MHz and 800 MHz were globally fit to yield the parameters listed above. Uncertainties in peak intensities were estimated using the variance for non-exchanging peaks, signal to noise, and duplicate points. Errors for rate constants and populations were estimated by the jackknife method.

Supplementary Note 1: The lack of dispersion at lower temperatures and a global increase in R_{ex} for WT EAdk to 2 Hz at 40 °C indicates that Mg^{2+} has a dramatic impact on the rate of lid-opening. 20°C , 30°C, 40°C.

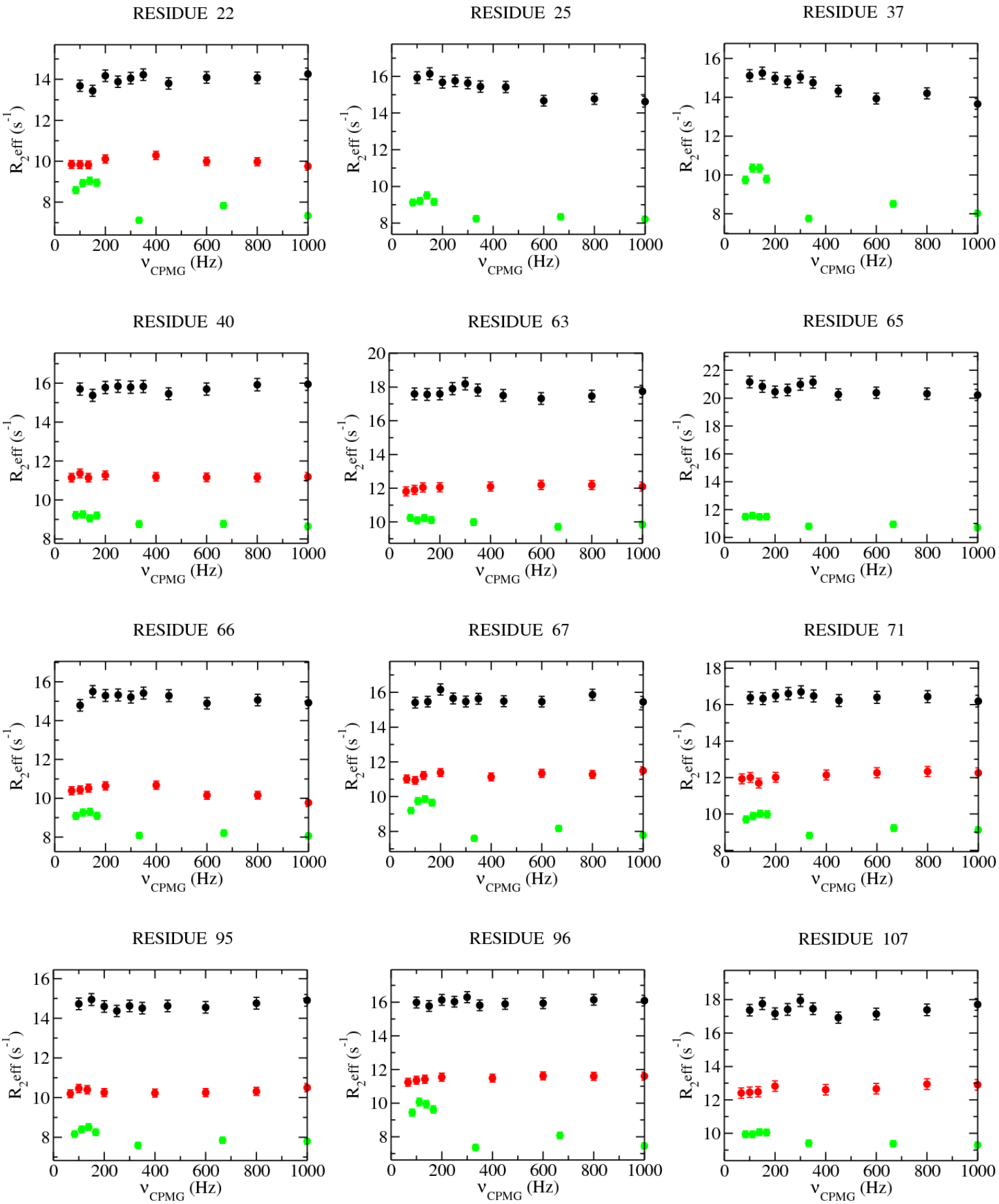

Nature Structural and Molecular Biology: doi:10.1038/nsmb.2941

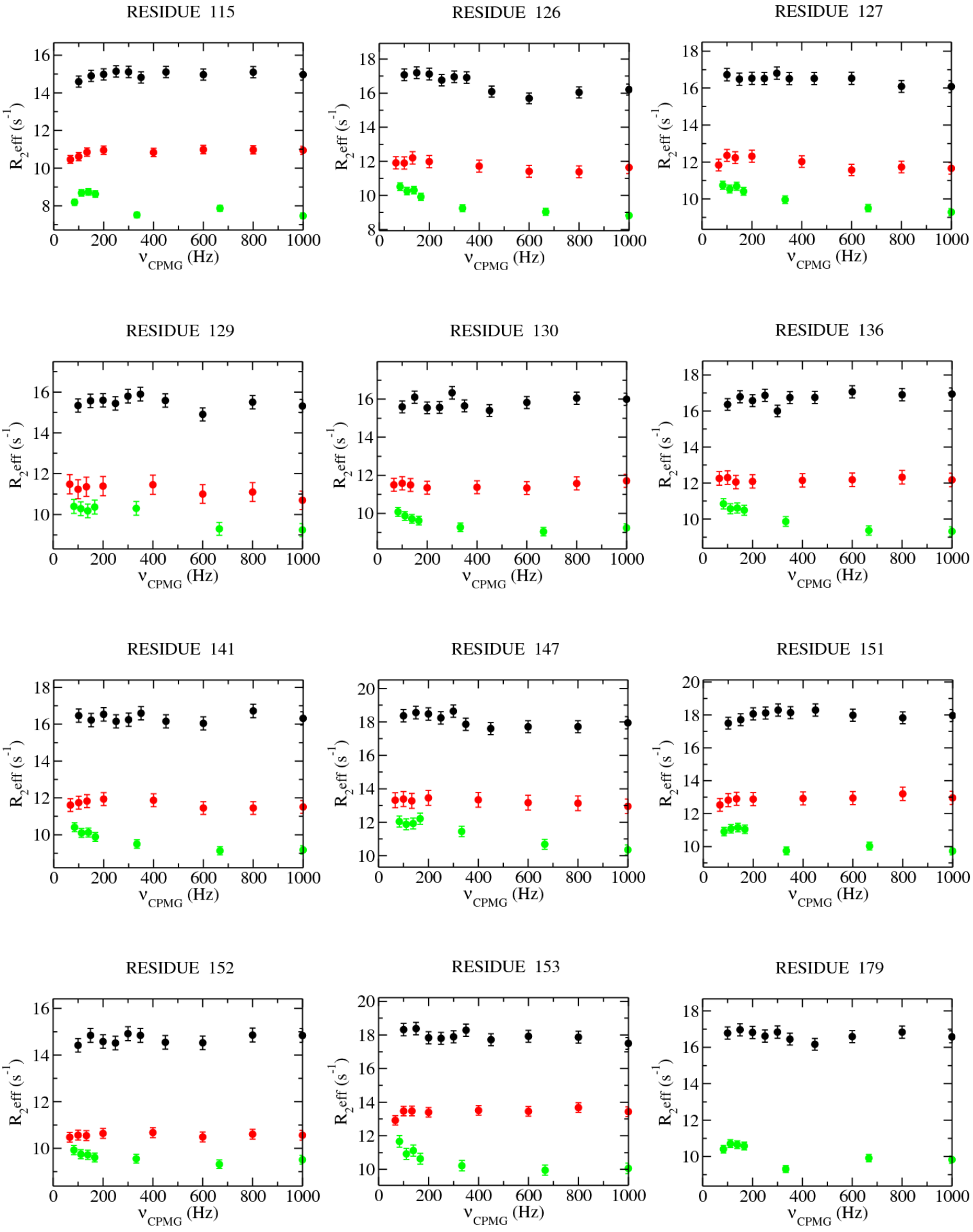

Nature Structural and Molecular Biology: doi:10.1038/nsmb.2941

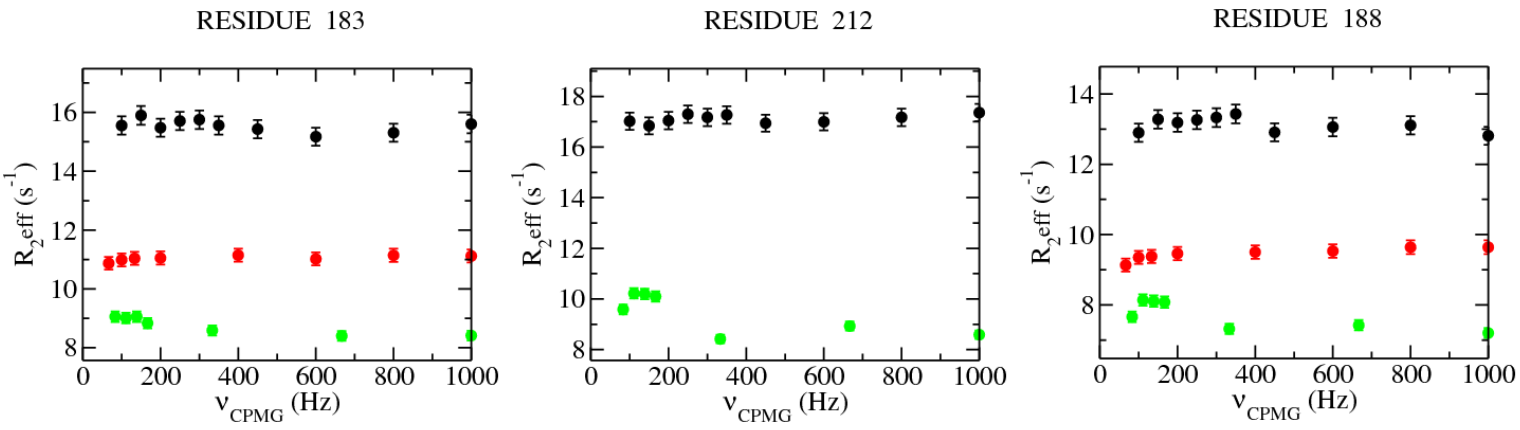

^{15}N-CPMG relaxation dispersion curves for residues reporting on lid-opening/closing with 20 mM nucleotides, 100 mM Tris pH 7, 50 mM NaCl, 5mM EDTA, and 2 mM WT EAdk at 20°C (black), 30°C (red), and 40°C (green). Linear extrapolation of the relaxation-dispersion curves at 40°C to the y-axis indicates a lid-opening rate of approximately 2 ± 1 s^{-1}.

Supplementary Note 2: Replacement of Mg^{2+} with Ca^{2+} during EAdk turnover does not significantly affect the rates of lid-opening/closing.

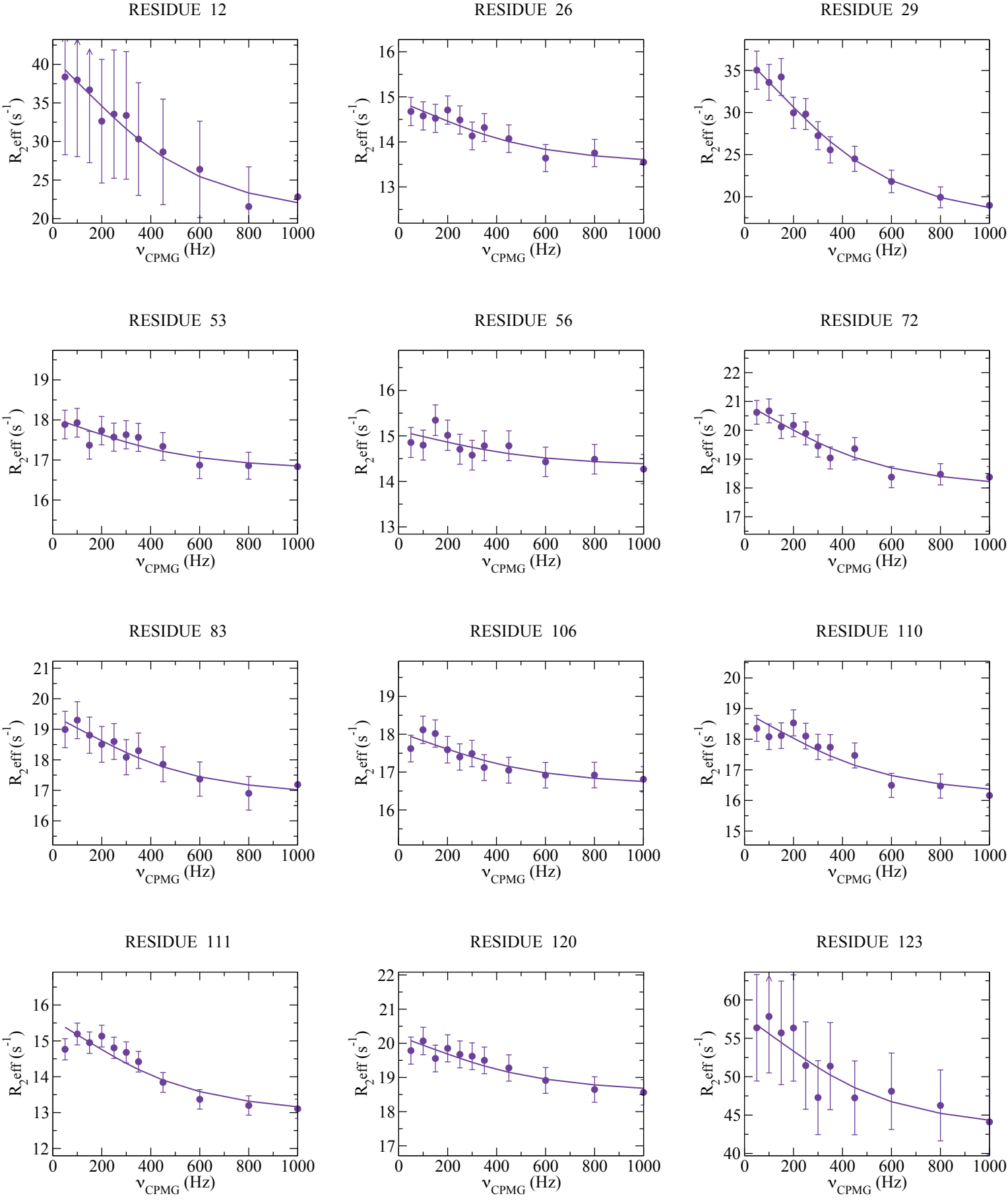

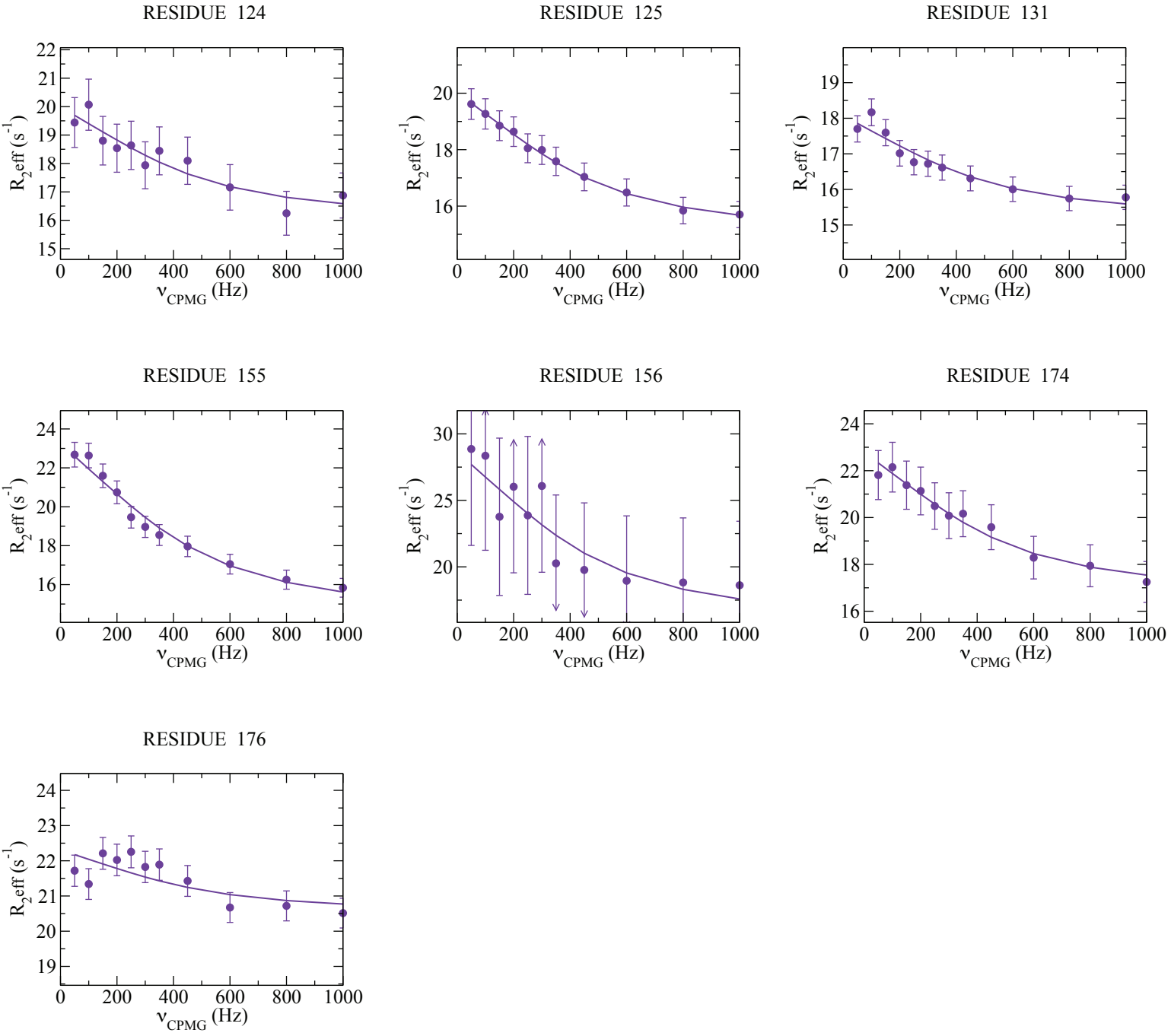

^{15}N-CPMG relaxation dispersion curves for residues reporting on lid-opening/closing with 20 mM nucleotides, 20 mM Mg^{2+} or Ca^{2+}, 100mM Tris pH 7, 50 mM NaCl, and 2 mM EAdk at 25°C. Data were globally fit to the general form of the Carver-Richards equation (Davis et al.) and yielded a k_{ex} of 1630 ± 30 s^{-1} and a closed population of 0.87 ± 0.05 with Mg^{2+} and a k_{ex} of 2870 ± 160 s^{-1} and a closed population of 0.87 ± 0.05 with Ca^{2+}.

Supplementary Note 3: Despite a 10^3 fold decrease in the rate of turnover, the rates of lid-opening/closing for the R150K mutant are very similar to WT EAdk.

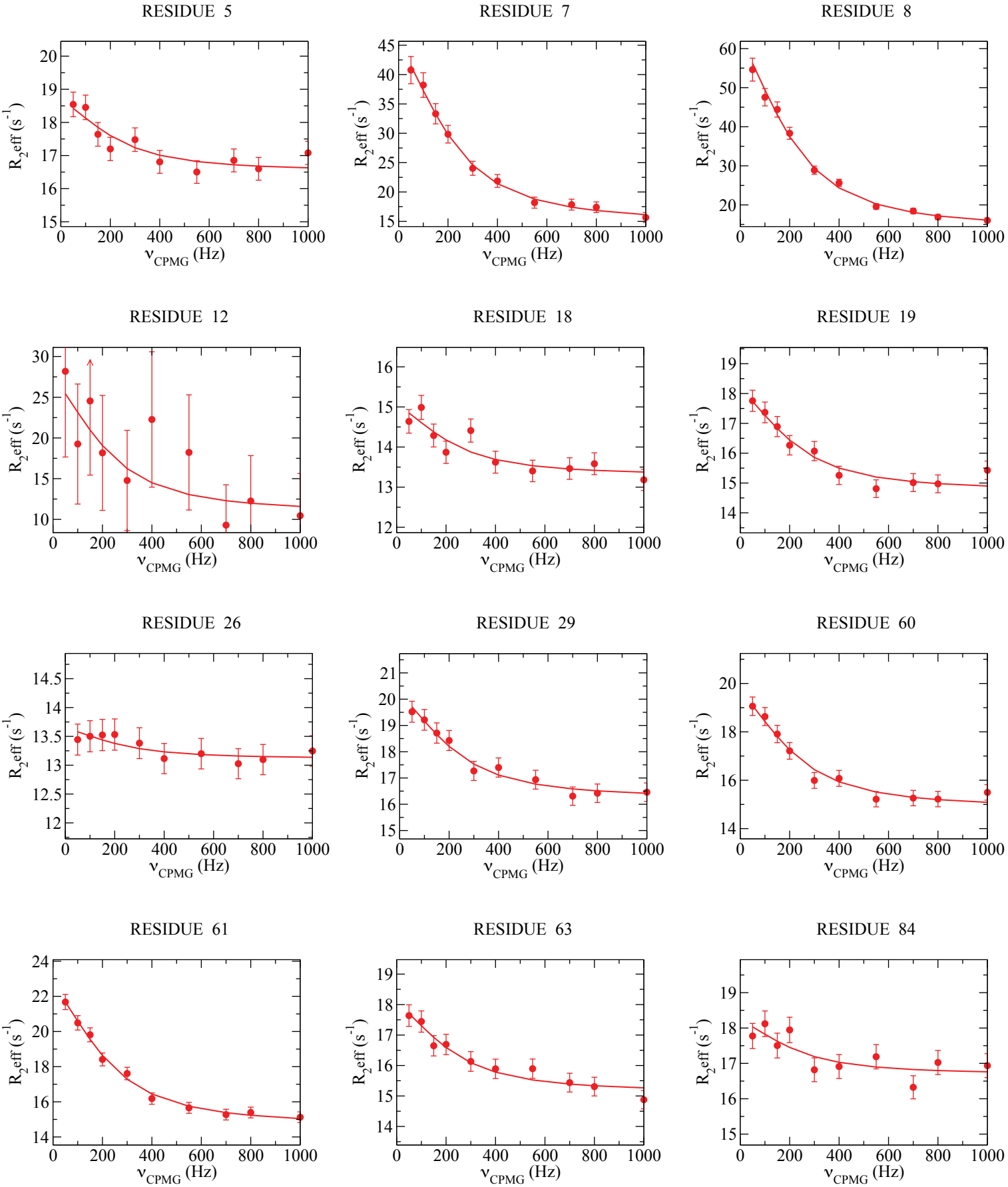

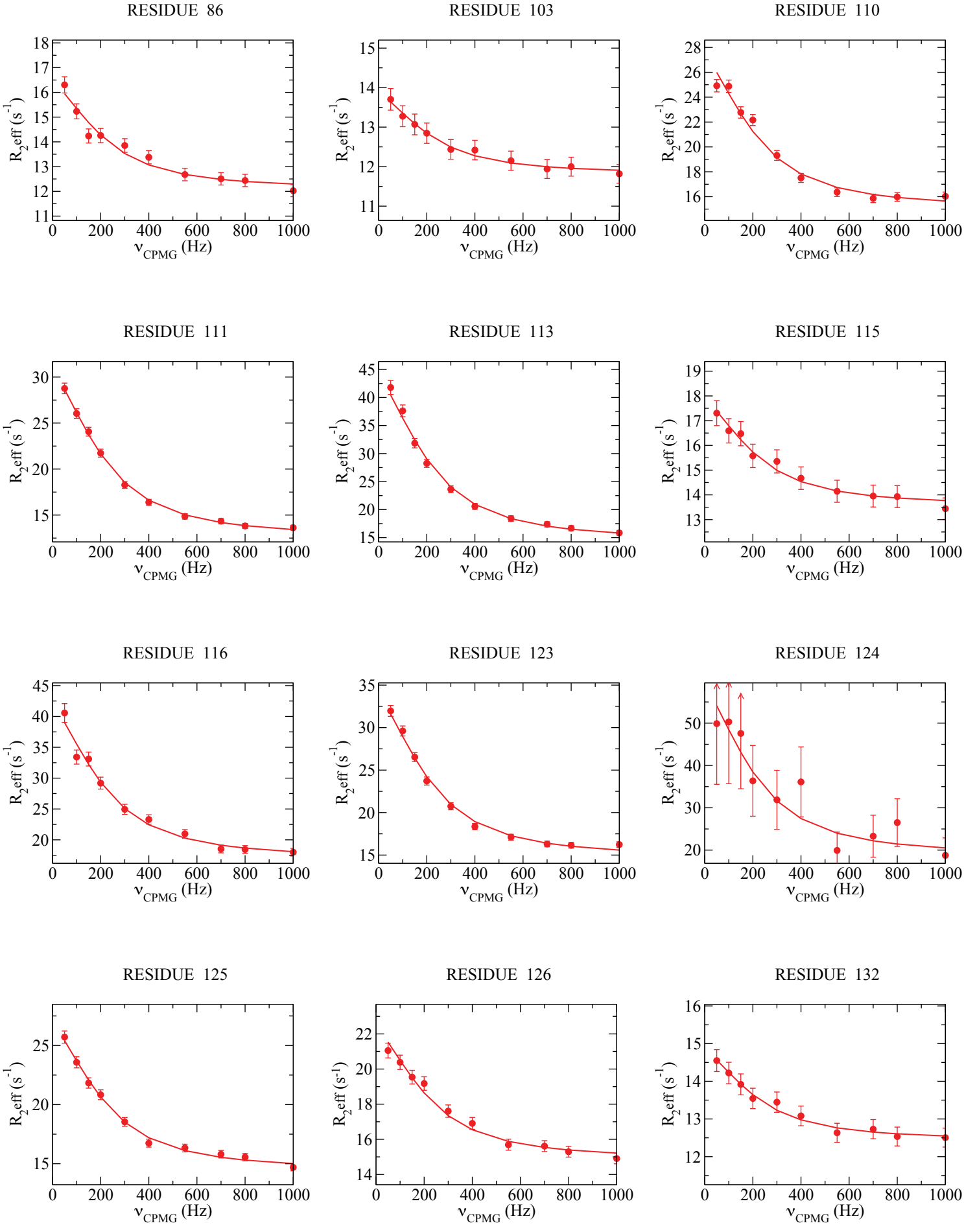

Nature Structural and Molecular Biology: doi:10.1038/nsmb.2941

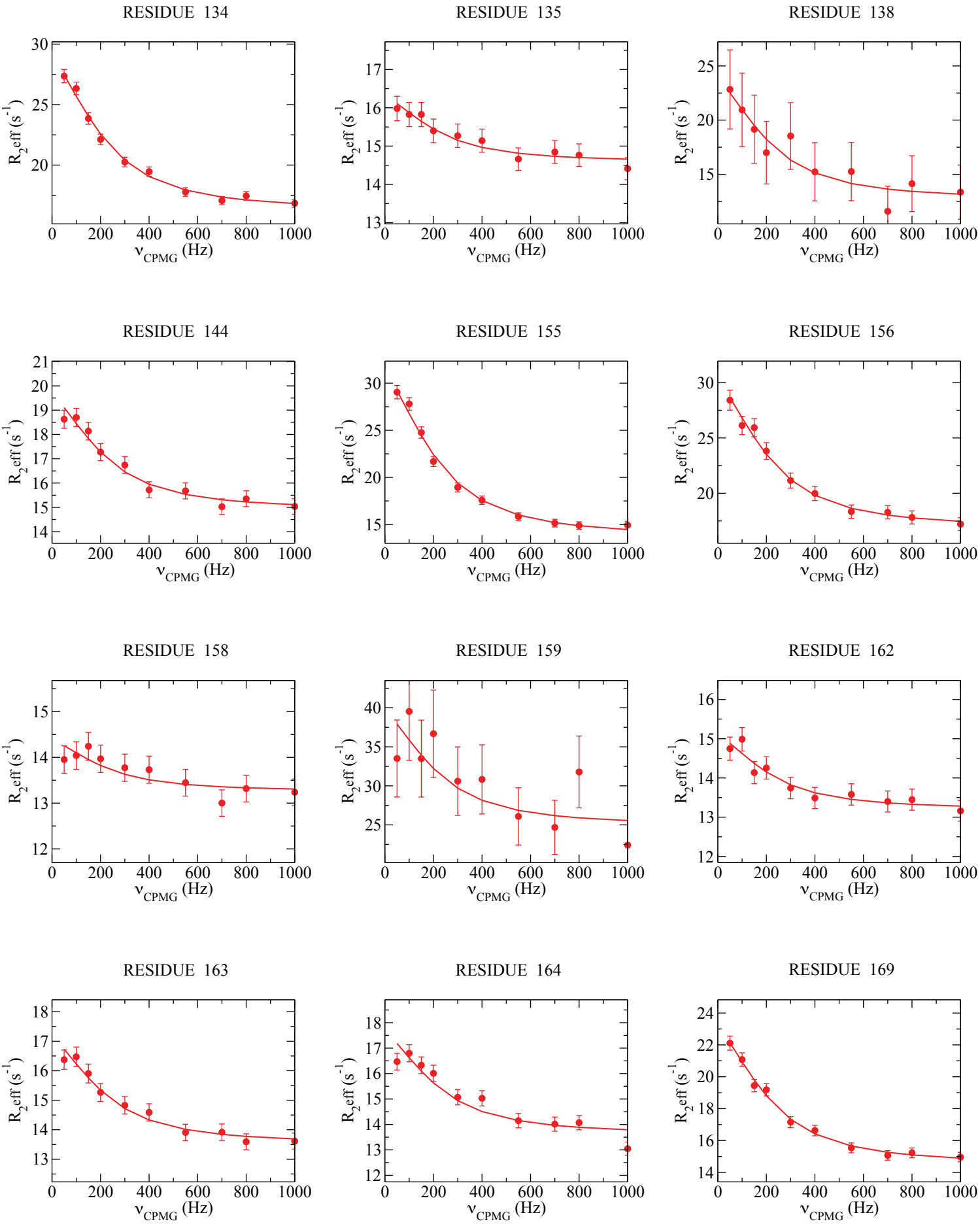

Nature Structural and Molecular Biology: doi:10.1038/nsmb.2941

RESIDUE 170

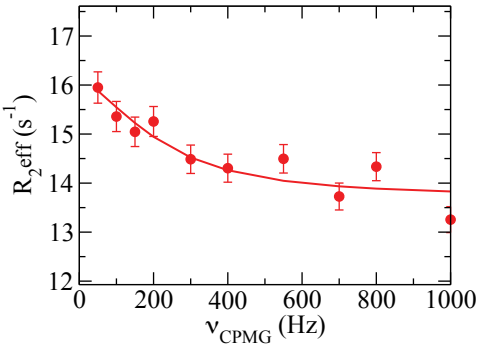

RESIDUE 171

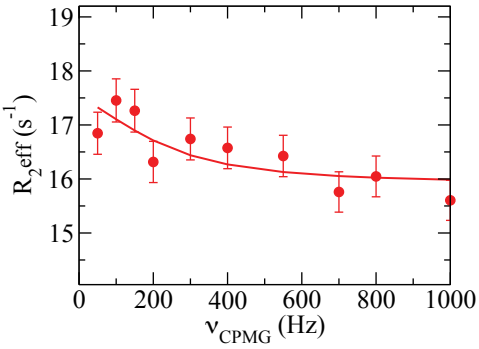

RESIDUE 173

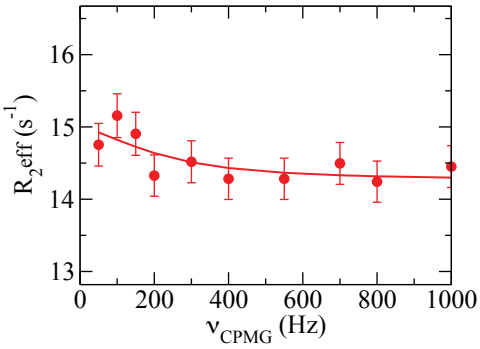

RESIDUE 174

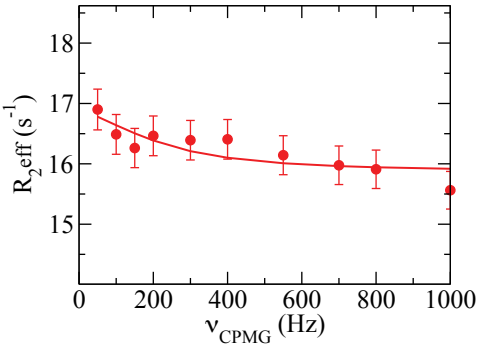

RESIDUE 175

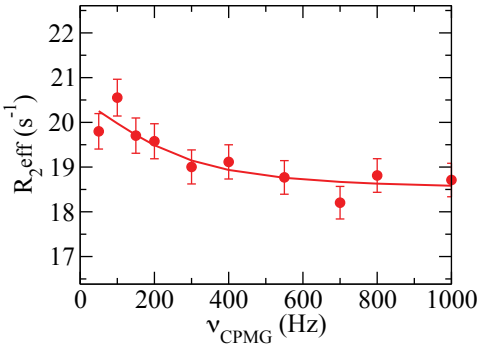

RESIDUE 176

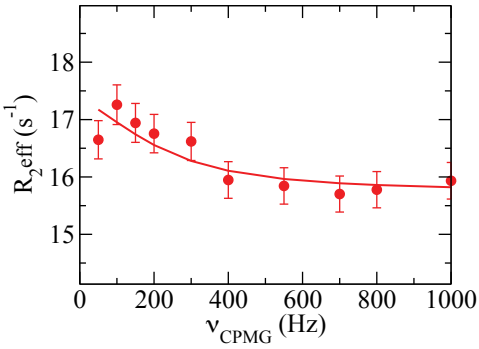

RESIDUE 178

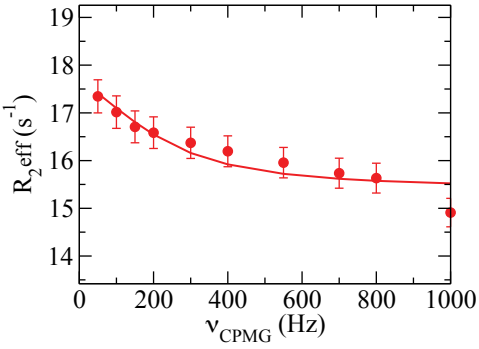

RESIDUE 183

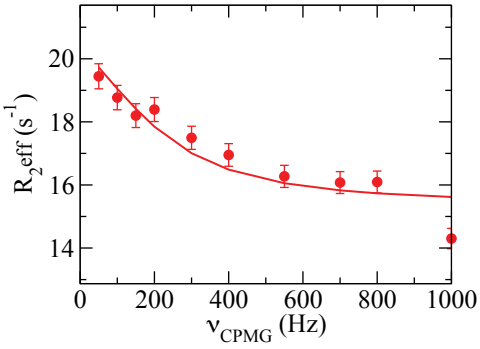

RESIDUE 185

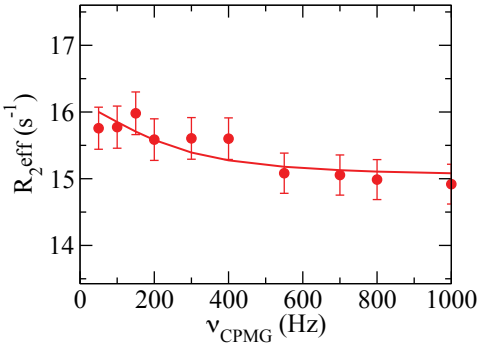

RESIDUE 187

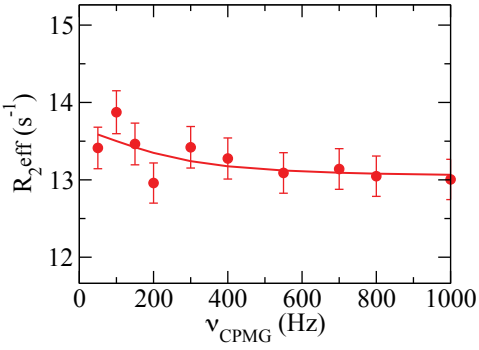

RESIDUE 195

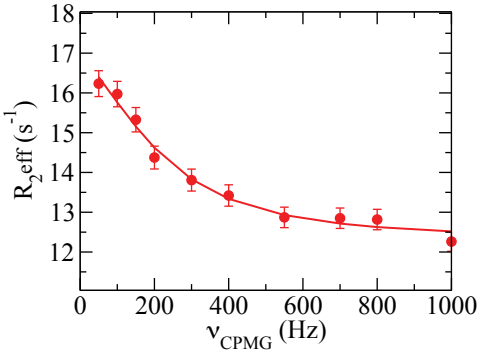

RESIDUE 198

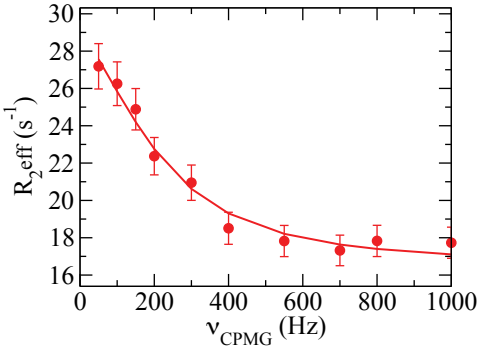

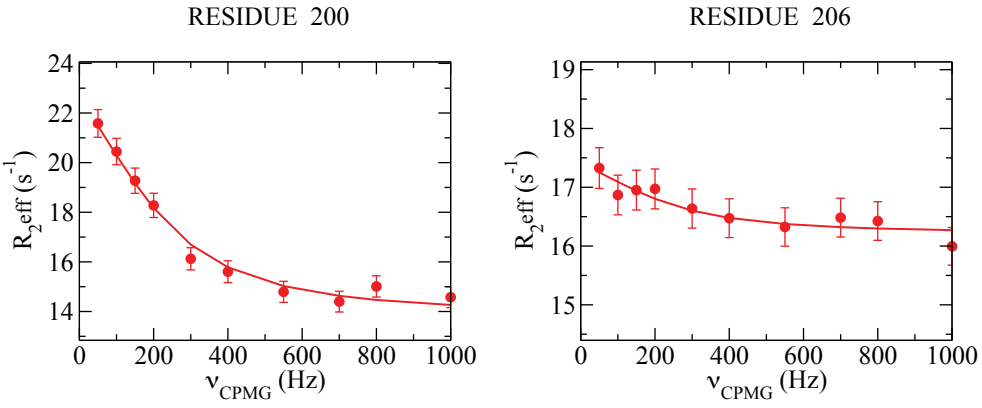

^{15}N-CPMG relaxation dispersion curves for residues reporting on lid-opening/closing with 20 mM nucleotides, 20 mM Mg^{2+}, 100 mM Tris pH 7, 50 mM NaCl, and 2 mM WT or R150K EAdk protein at 25°C. Data were globally fit to the general form of the Carver-Richards equation (Davis et al.) and yielded a k_{ex} of 1630 ± 30 s^{-1} and a major or closed population of 0.87 ± 0.05 for WT EAdk and a k_{ex} of 1500 ± 30 s^{-1} and closed population of 0.80 ± 0.05 for the R150K mutant protein. Note that the residue number labeling in the CPMG dispersion profiles is according to the true E.coli Adk sequence.

Nature Structural and Molecular Biology: doi:10.1038/nsmb.2941

Supplementary Note 4: Similar to WT EAdk, the rate of lid-opening for the phosphoryl-transfer impaired R150K mutant is also significantly slower without Mg^{2+}. **10°C , 20°C, 40°C**

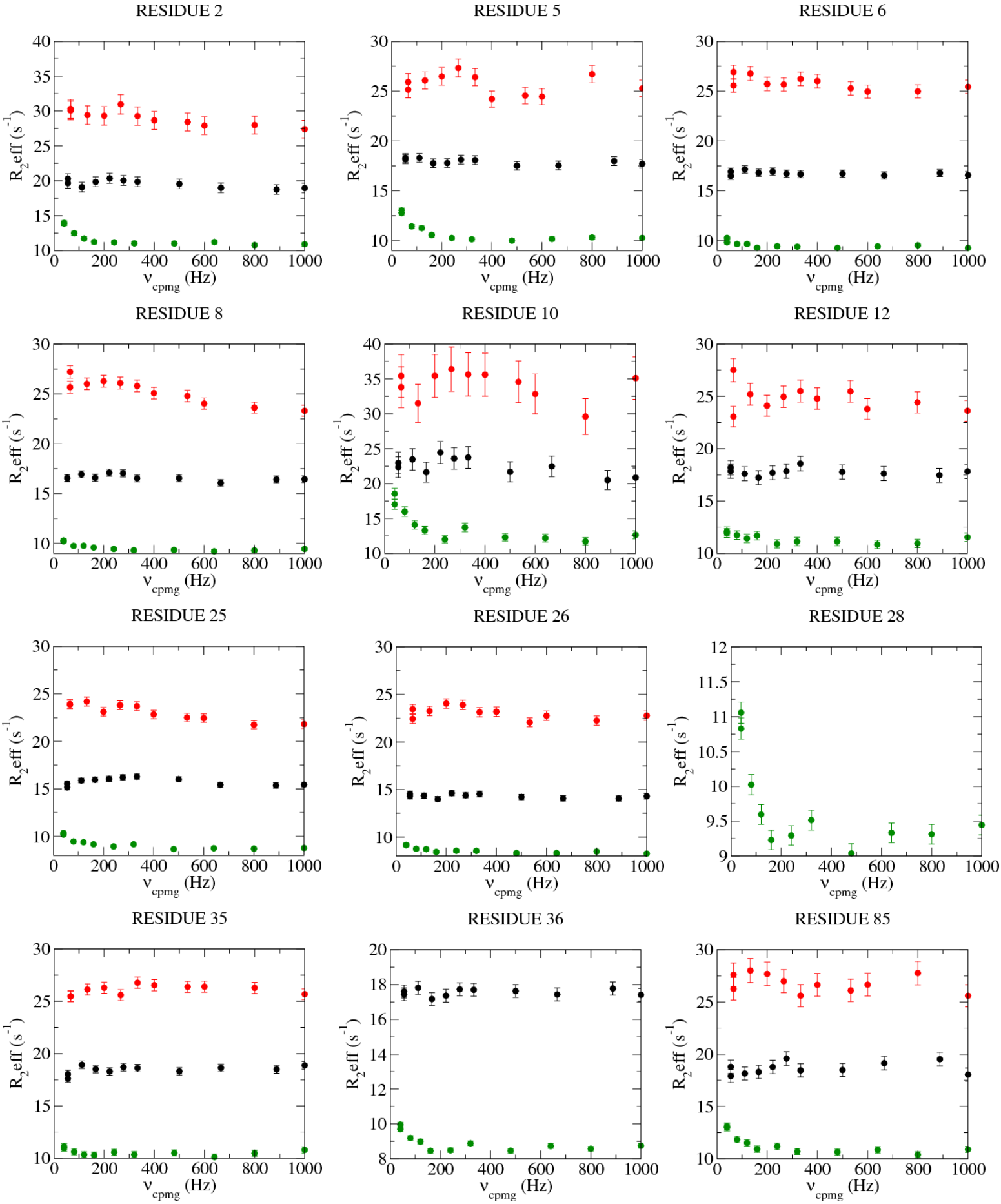

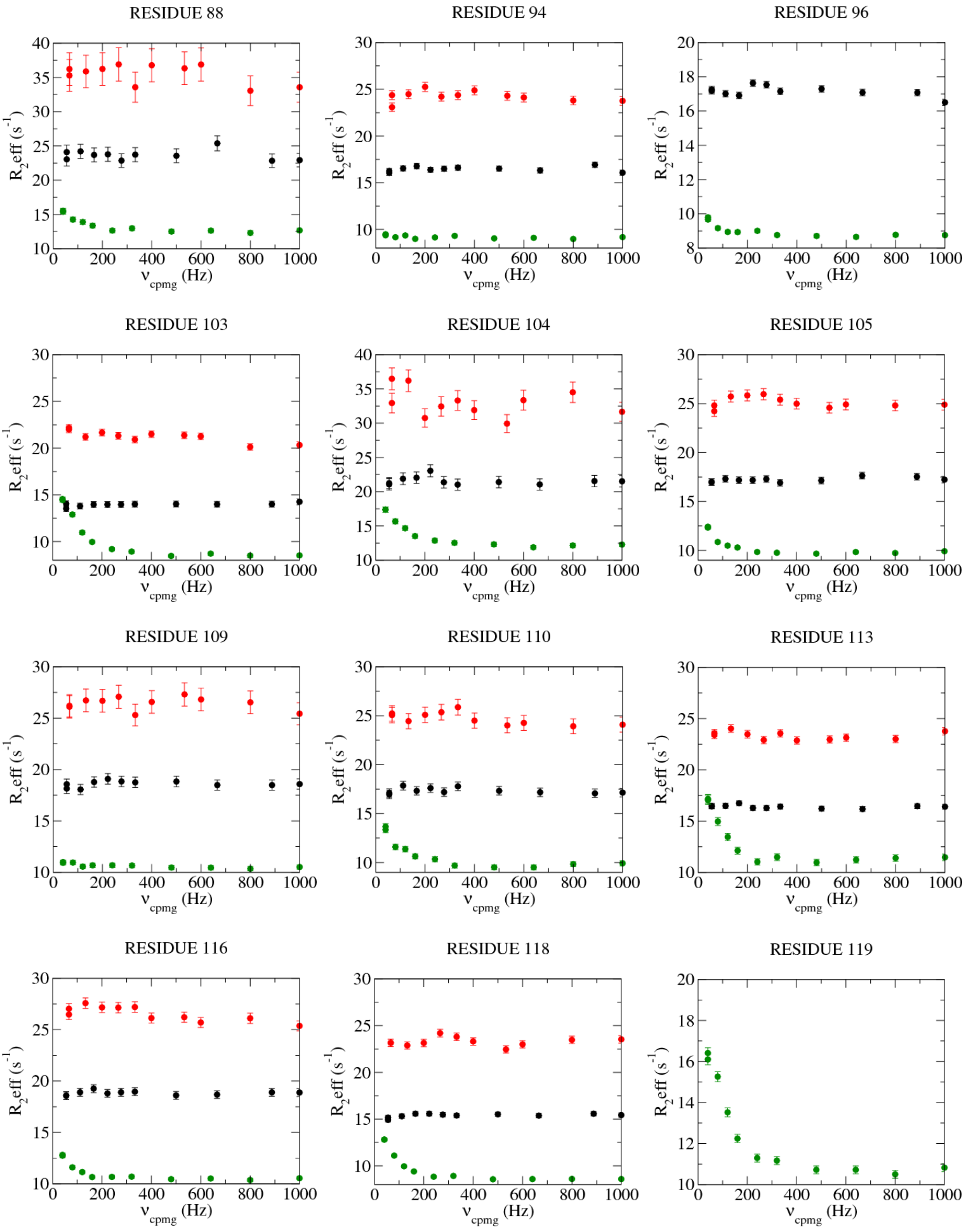

Nature Structural and Molecular Biology: doi:10.1038/nsmb.2941

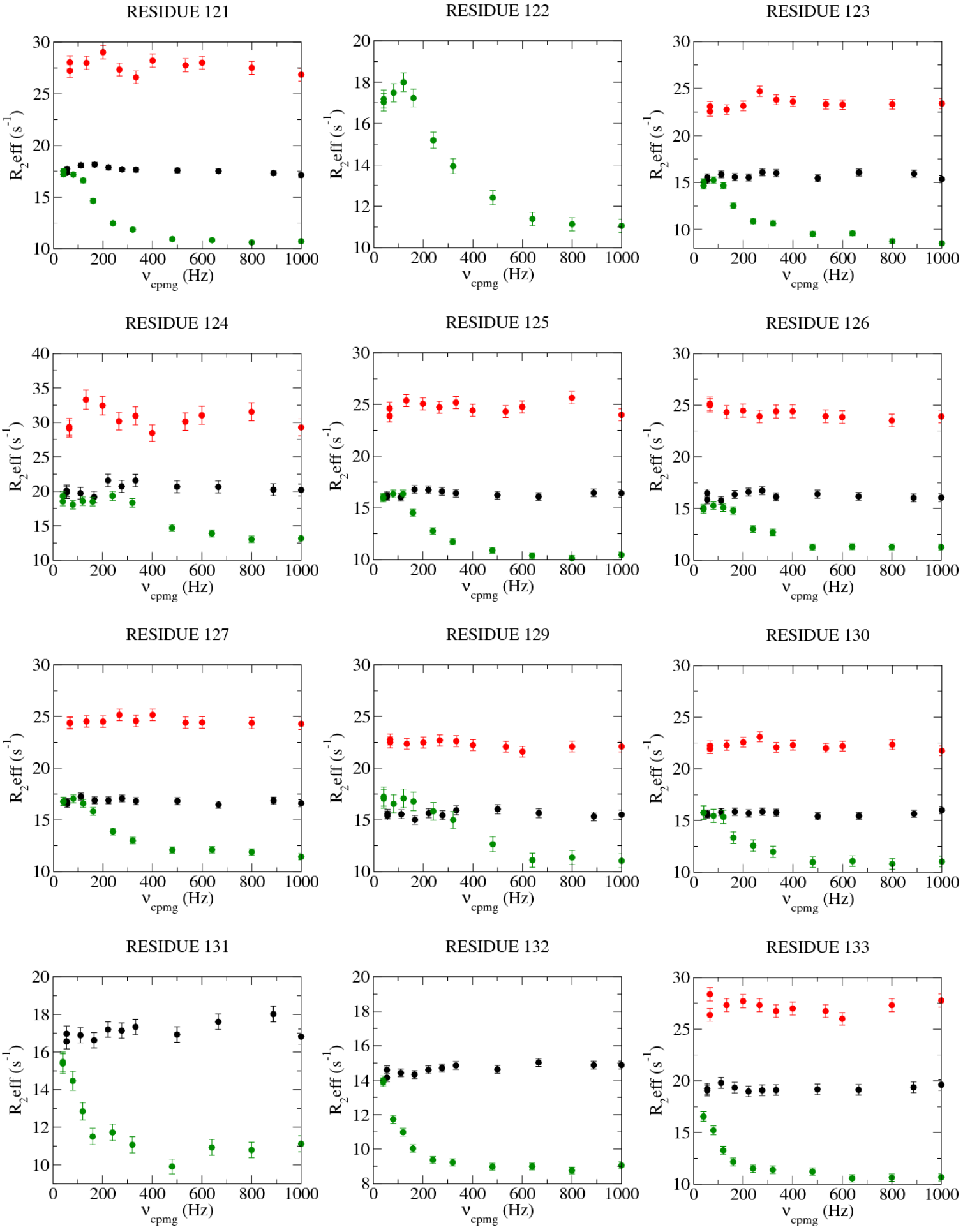

Nature Structural and Molecular Biology: doi:10.1038/nsmb.2941

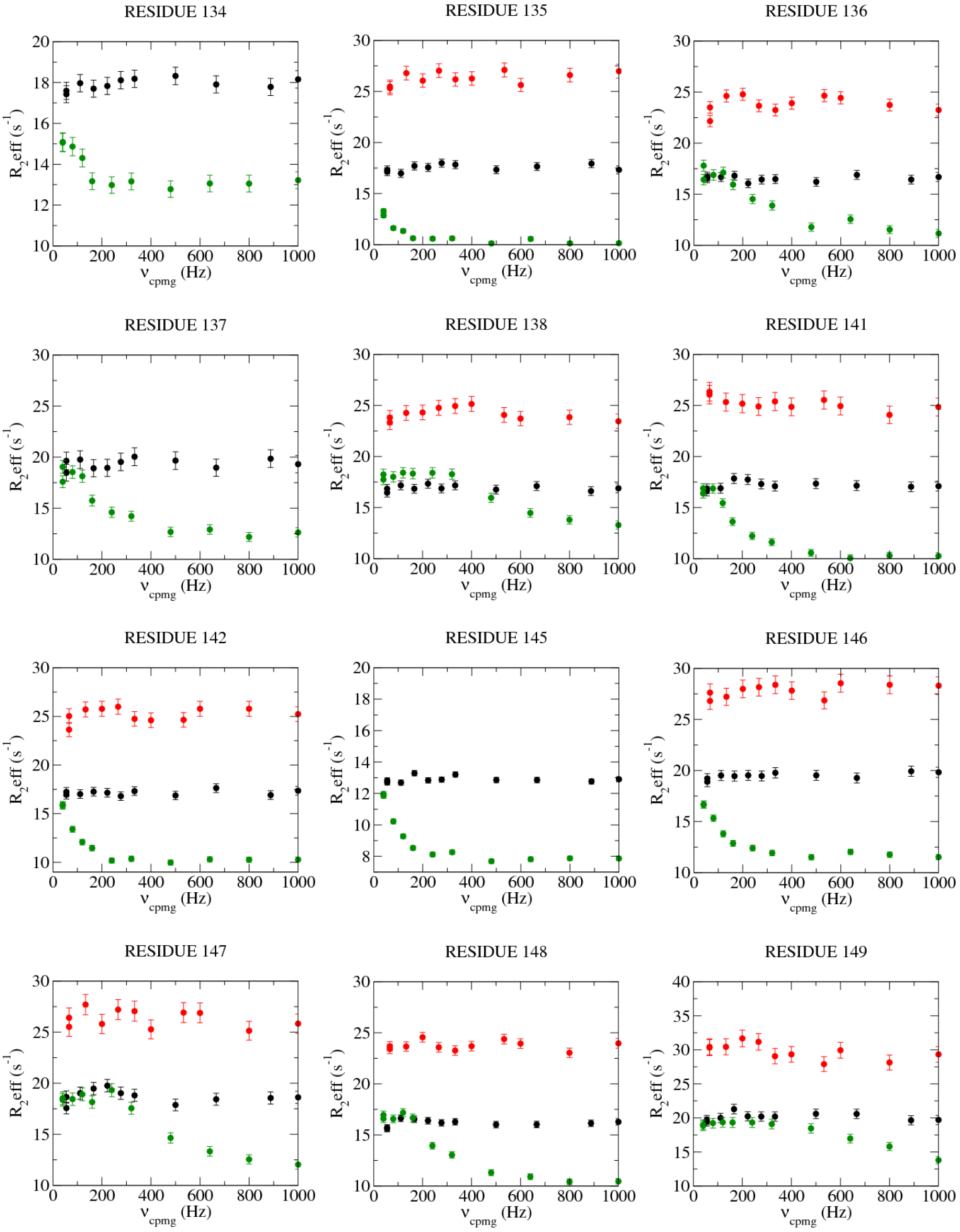

Nature Structural and Molecular Biology: doi:10.1038/nsmb.2941

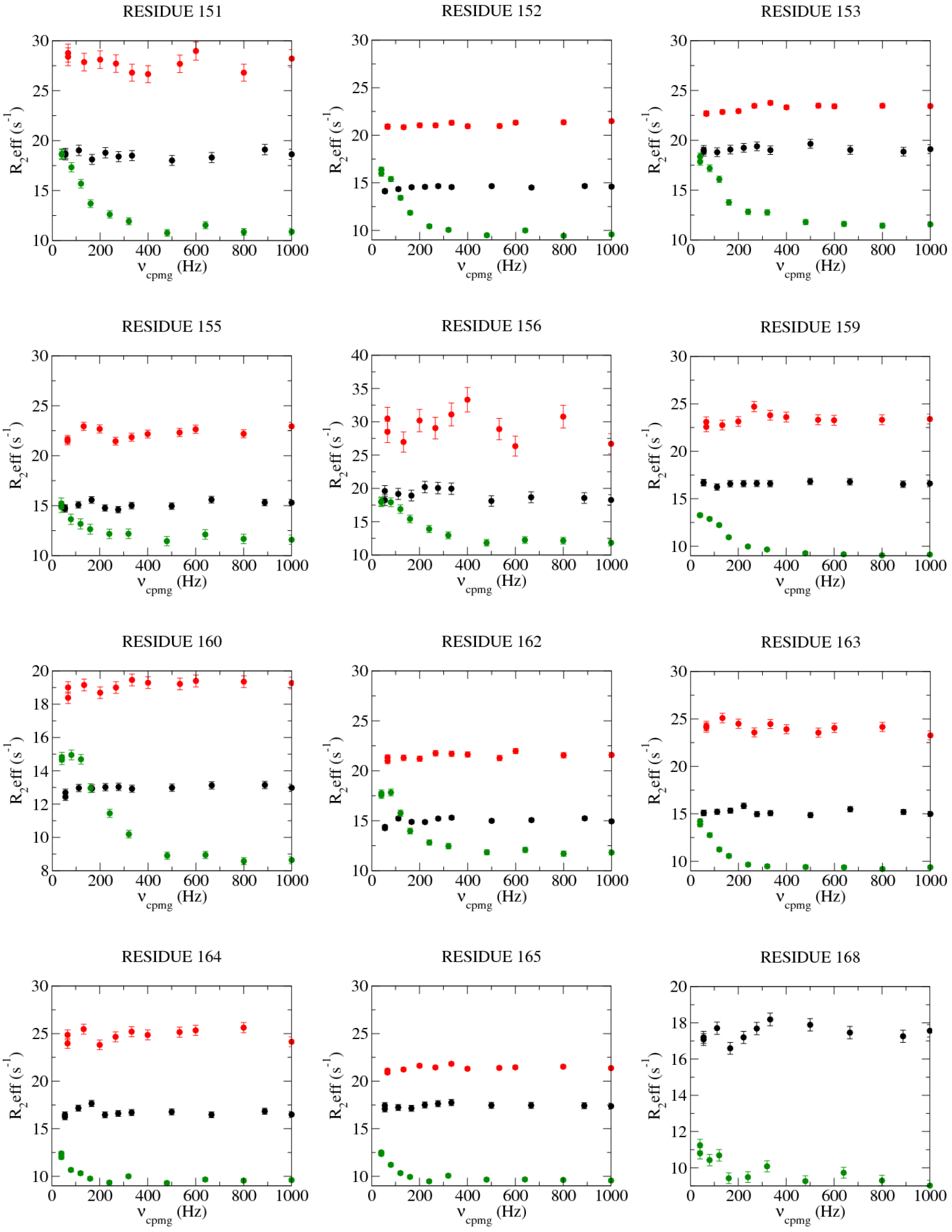

Nature Structural and Molecular Biology: doi:10.1038/nsmb.2941

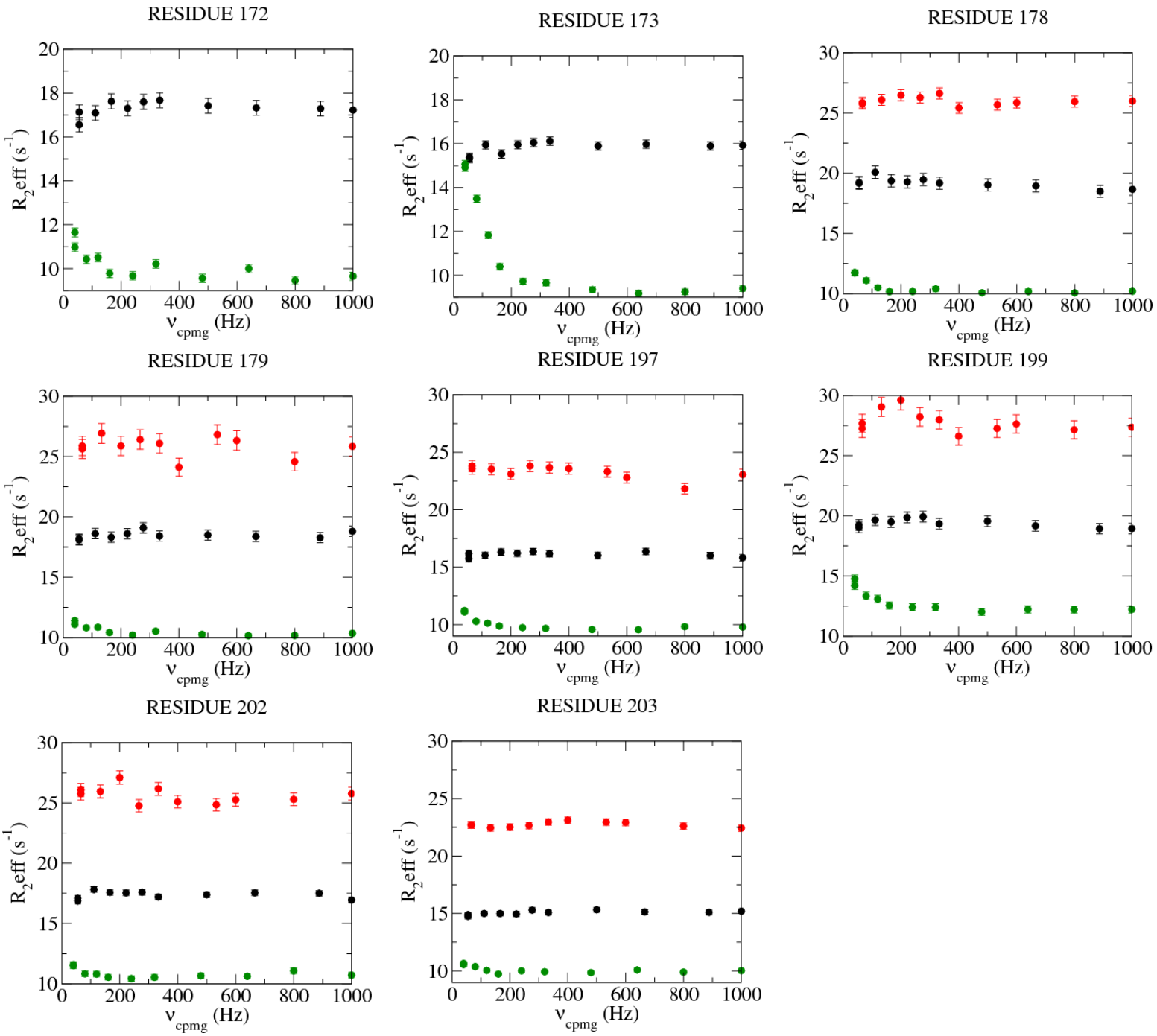

^{15}N-CPMG relaxation dispersion curves for residues reporting on lid-opening with 20 mM nucleotides,100 mM Tris pH 7, 50 mM NaCl, 5mM EDTA, and 2 mM EAdk R150K at 10^{o}C (red), 20^{o}C (black), and 40^{o}C (green).